Compact star-forming galaxies preferentially quenched to become PSBs in $z < 1$ clusters

Miguel Socolovsky,[1]★ David T. Maltby,[1] Nina A. Hatch [ID],[1] Omar Almaini [ID],[1] Vivienne Wild,[2] William G. Hartley,[3] Chris Simpson[4] and Kate Rowlands [ID][5]

[1]*School of Physics and Astronomy, University of Nottingham, Nottingham NG7 2RD, UK*
[2]*School of Physics and Astronomy, University of St Andrews, North Haugh, St Andrews, KY16 9SS, UK*
[3]*Department of Physics and Astronomy, University College London, 3rd Floor, 132 Hampstead Road, London NW1 2PS, UK*
[4]*Gemini Observatory, Northern Operations Center, 670 N. A'ohoku Place, Hilo, HI 96720-2700, USA*
[5]*Department of Physics and Astronomy, Johns Hopkins University, Bloomberg Center, 3400 N. Charles St., Baltimore, MD 21218, USA*

ABSTRACT

We analyse the structure of galaxies with high specific star formation rate (SSFR) in cluster and field environments in the redshift range $0.5 < z < 1.0$. Recent studies have shown that these galaxies are strongly depleted in dense environments due to rapid environmental quenching, giving rise to post-starburst galaxies (PSBs). We use effective radii and Sérsic indices as tracers of galaxy structure, determined using imaging from the UKIDSS Ultra Deep Survey (UDS). We find that the high-SSFR galaxies that survive into the cluster environment have, on average, larger effective radii than those in the field. We suggest that this trend is likely to be driven by the most compact star-forming galaxies being preferentially quenched in dense environments. We also show that the PSBs in clusters have stellar masses and effective radii that are similar to the missing compact star-forming population, suggesting that these PSBs are the result of size-dependent quenching. We propose that both strong stellar feedback and the stripping of the extended halo act together to preferentially and rapidly quench the compact and low-mass star-forming systems in clusters to produce PSBs. We test this scenario using the stacked spectra of 124 high-SSFR galaxies, showing that more compact galaxies are more likely to host outflows. We conclude that a combination of environmental and secular processes is the most likely explanation for the appearance of PSBs in galaxy clusters.

Key words: galaxies: clusters: general – galaxies: evolution – galaxies: high-redshift – galaxies: structure.

1 INTRODUCTION

In the local Universe the most massive galaxies are passive (PAS) and elliptical, while low-mass galaxies tend to be star-forming (SF) and have disc-dominated morphologies. Several studies at high red-shift show that massive PAS galaxies are already in place at $z = 2$ (van der Wel et al. 2008; Bamford et al. 2009; Baldry et al. 2012). In contrast, the observed number of quenched low-mass galaxies increases towards the present day (Drory et al. 2009; Baldry et al. 2012; Moutard et al. 2016, 2018). This downsizing in the PAS population is generally associated with environmental quenching, and has been measured up to $z \sim 1$ (Muzzin et al. 2013; Tomczak et al. 2014; Socolovsky et al. 2018). These evolutionary trends are consistent with galaxies in high-density environments being more likely to be PAS regardless of their stellar mass (Balogh et al. 1997;

Baldry et al. 2006; Yang, Mo & van den Bosch 2009; Peng et al. 2010; Hartley et al. 2013).

There are various proposed mechanisms to explain environmental quenching, but consensus has not yet been reached on which are the dominant processes. Interactions with the intra-cluster medium (ICM), such as strangulation (Larson, Tinsley & Caldwell 1980) or ram-pressure stripping (Gunn & Gott 1972), are some of the preferred mechanisms to explain how SF galaxies are deprived of their gas reservoirs and subsequently quench. Alternative mechanisms invoke galaxy–galaxy interactions, such as mergers, harassment, or tidal stripping (Moore et al. 1996; Toomre & Toomre 1972; Faber 1973), which are examples of other processes typically associated with high- and intermediate-density environments.

Galaxy structure provides a window into the evolutionary history of galaxies, so studying the structure of different galaxy populations can help to disentangle the driving quenching mechanisms. Gravitational interactions (including major mergers) may induce the migration of gas and stars towards the galaxy centre, producing

★ E-mail: miguel.socolovsky@nottingham.ac.uk

more compact and concentrated light profiles. This contrasts with the faded discs generated when the gas is ram-pressure stripped via interaction with the ICM. The environmental dependence of the galaxy stellar-mass–size relation for early-type galaxies has been extensively studied in the past. Cooper et al. (2012) and Lani et al. (2013) used local density as a tracer of environment at $z > 1$, and found that red sequence galaxies at fixed stellar mass present larger radii in high-density environments. A different type of study, i.e. comparing cluster and field galaxies at $z = 1.6$, also showed that early-type galaxies are larger in the cluster environment (Papovich et al. 2012). In contrast, at lower redshift, Kelkar et al. (2015) found no significant difference between cluster and field galaxies at $z \sim 0.6$. They concluded that the size evolution in the field might have caught up with the cluster, erasing the observed differences at higher redshifts.

Previous studies seem to agree that the growth in size of passive galaxies in dense environments is driven by dry merging and tidal interactions (e.g. Cooper et al. 2012; Lani et al. 2013). However, not much work has been done on how the mass–size relation of SF galaxies is affected by environment at high redshift. In the low-redshift Universe, some authors have found that late-type galaxies are larger in the field than in galaxy clusters (Maltby et al. 2010; Cebrián & Trujillo 2014). In this paper, we extend the study of the mass–size relation of SF galaxies in different environments to $z = 1$.

The most depleted population in clusters are those with low stellar masses and high specific star formation rates (SSFRs). In Socolovsky et al. (2018), we showed that these high-SSFR galaxies are likely to evolve into low-mass post-starbursts (PSBs) in dense environments at $0.5 < z < 1.0$. By studying the stellar-mass function, we found a significant excess of low-mass PSBs in clusters. The mass distribution of these recently quenched galaxies in clusters is only comparable to the mass function of young, high-SSFR galaxies (SF1 galaxies) in the field. Therefore, SF1 galaxies are likely to be the progenitors of PSBs in dense environments, where they experience rapid environmental quenching. In this paper, we investigate the quenching mechanisms by studying the stellar-mass–size relation of PSBs and their progenitors, SF1 galaxies.

The structure of the paper is as follows. In Section 2, we present our data, the classification method and a description of how structural parameters are measured from ground-based imaging. We also present a brief description of the cluster-finding algorithm, developed in Socolovsky et al. (2018). We present our results in Section 3 and discuss their possible implications in Section 4. Finally, our conclusions are listed in Section 5. Throughout this paper, we use AB magnitudes measured using 2 arcmin apertures, and assume a ΛCDM cosmology with the following parameters: $\Omega_M = 0.3$, $\Omega_\Lambda = 0.7$, and $H_0 = 70 \, \text{km s}^{-1} \, \text{Mpc}^{-1}$.

2 DATA SETS AND GALAXY CLASSIFICATION

2.1 Galaxy catalogue

The galaxy catalogue we use is based on the 8th data release of the UDS (Almaini et al., in preparation), with coverage in the near-infrared to 5σ depths measured in 2 arcmin apertures of $J = 24.9$, $H = 24.2$, and $K = 24.6$. Deep optical imaging is also available from the Subaru *XMM–Newton* Deep Survey (SXDS; Furusawa et al. 2008; Ueda et al. 2008), with 5σ depths of $B = 27.6$, $V = 27.2$, $R = 27.0$, $i' = 27.0$, and $z' = 26.0$. Deep *U*-band imaging is provided by the Canada–France–Hawaii Telescope (CFHT), to a depth of $U = 26.75$ to 5σ and the *Spitzer* Legacy Program (SpUDS)

provides $[3.6] = 24.2$ and $[4.5] = 24.0$ at 5σ. The combined area, after masking, covers $\sim$0.62 square degrees.

The catalogue is limited to $K < 24.3$ which ensures a 95 per cent completeness (Hartley et al. 2013). The missing 5 per cent corresponds mainly to low surface brightness galaxies. This leads to a catalogue with 23 398 galaxies at $0.5 < z < 1.0$. Stars are identified and removed according to the method described in Simpson et al. (2013).

2.2 Photometric redshifts and stellar masses

We use the photometric redshifts derived by Simpson et al. (2013) based on the UDS DR8 photometry. They use the EAZY photometric-redshift code (Brammer, van Dokkum & Coppi 2008) to fit template spectra to the U, B, V, R, i', z', J, H, K, 3.6 μm, and 4.5μm photometry. Approximately 1500 spectroscopic redshifts from the UDSz (ESO Large Programme, Almaini et al., in preparation) and 3500 from the literature (Simpson et al. 2012) were used to test these photometric redshifts. The measured median absolute deviation is $\sigma_{NMAD}(\Delta z/(1 + z)) \sim 0.023$ up to $z = 1.0$, with < 4 per cent outliers, defined as sources with $\Delta z/(1 + z) > 5\sigma_{NMAD}$, once AGNs are removed. Galaxy redshifts were fixed to the spectroscopic values, where available, otherwise photometric redshifts were assumed.

The stellar masses are also calculated in Simpson et al. (2013) by fitting a grid of synthetic spectral energy distributions (SEDs) to the 11-band photometry, built using Bruzual & Charlot (2003) stellar population synthesis models and using the Chabrier (2003) initial mass function.

2.3 Galaxy classification and SSFRs

We use the galaxy classification described in Wild et al. (2016) which is based on a principal component analysis (PCA) outlined in Wild et al. (2014). See these two papers for a more detailed description of the method. We provide here a brief overview of the key features as well as describe the galaxy classes we use.

Three eigenspectra are determined using a PCA on a grid of 44 000 model SEDs, using the stellar population synthesis models from Bruzual & Charlot (2003). The coefficients that quantify the contribution of each of these eigenspectra in order to reproduce one galaxy SED are named 'supercolours'. The first supercolour, $SC1$, modifies the red–blue slope and traces the R-band weighted mean stellar age or SSFR. Supercolour $SC2$ alters the strength of the Balmer break and correlates with the fraction of the stellar mass formed in bursts during the last billion years, and also traces metallicity. Supercolour $SC3$ affects the shape of the SED around 4000 Å and is used to break the degeneracy between metallicity and the fraction of the stellar mass formed during the last Gyr.

The PCA allows us to derive other physical properties of galaxies, which are obtained from the grid of models described above. Hence, the SSFRs we use in this work are computed using the supercolour method (see Wild et al. 2016). Although the PCA can provide stellar masses, we choose to use the masses from Simpson et al. (2013) derived using SED fitting. These masses are better constrained as all 11 photometric bands are used, rather than the 8 used in the PCA (see Wild et al. 2016, for more details).

The galaxy classification is based on the position of galaxies in SC–SC diagrams (typically SC1–SC2 and SC1–SC3) and the boundaries between populations are determined empirically using model SEDs and spectroscopy (see Wild et al. 2014). This method divides the population into SF, PAS, PSB, metal-poor and dusty

galaxies (the last two are excluded from our sample). Additionally, the SF population is also divided into three sub-populations of decreasing SSFR: SF1, SF2, and SF3. The method has also been spectroscopically confirmed (Wild et al. 2014; Maltby et al. 2016).

The PCA is applied to a catalogue with a magnitude limit of $K < 24$. This catalogue is slightly more conservative than the one described in Section 2.1, which reduces the noise in the supercolour determination (see Wild et al. 2016). This leads to 11, 625 SF1, 3, 486 SF2, 2, 055 SF3, 2, 206 PAS, and 418 PSBs in the redshift range $0.5 < z < 1.0$. We compute 90 per cent mass completeness limits for each galaxy type using the method of Pozzetti et al. (2010). The values of $\log M_{lim}/M_\odot$ to ensure a 95 per cent mass completeness at $z = 1$ are 9.0 for SF, 9.5 for PAS, and 9.3 for PSB galaxy populations.

2.4 Cluster and field samples

The cluster and field samples are drawn from Socolovsky et al. (2018). The classification method is based on a friends-of-friends algorithm which runs on the K-band galaxy catalogue of the UDS. This algorithm depends on three parameters which are tested and optimized by running the algorithm on a mock catalogue which includes simulated galaxy clusters (we refer the reader to Socolovsky et al. 2018 for details).

The sample, consisting of 37 galaxy overdensities at $0.5 < z < 1.0$, is likely to be dominated by group-like structures ($\sigma_v = 300$–$500\,km\,s^{-1}$) combined with more massive galaxy clusters. For the purposes of this study, henceforth we refer to these overdensities collectively as 'clusters'. A threshold of at least 20 detected members is applied to ensure a high signal to noise (S/N; see Socolovsky et al. 2018). Every galaxy located within 1 Mpc from the projected centre of mass and $2.5\sigma_z$ [$\sigma_z = 0.023(1 + z)$] from the median redshift of the measured structure was included in the cluster sample to ensure membership completeness. These criteria are applied to both galaxies with and without spectroscopic redshifts for consistency. This cluster sample, therefore, contains contaminants from the field. The field sample is constructed using all the galaxies in the UDS field that were not associated with an overdensity, while forced to follow the redshift distribution of the cluster sample. In total the sample has 2 210 cluster galaxies and 13 837 in the field between $0.5 < z < 1.0$.

2.5 Galaxy size and Sérsic index from UDS DR11

Structural parameters (i.e. effective radius, R_e and Sérsic index, n) were determined using the K-band image from the UDS DR11 ($J = 25.6$, $H = 25.1$, $K = 25.3$; 5σ, AB). The software employed was GALAPAGOS (Barden et al. 2012), which makes use of GALFIT (Peng et al. 2002) in order to fit a Sérsic light profile (Sérsic 1968) to each galaxy in the UDS. We refer the reader to Almaini et al. (2017) for further details.

We rejected poor fits ($\chi_\nu^2 > 100$) which correspond to 1.7 per cent of our sample. Similarly, we rejected ∼7 per cent of galaxies where GALFIT did not converge to one solution. Most of these rejections correspond to objects with low surface brightness and near masked regions. The rejection rate was similar for SF, PAS, and PSB galaxies; and for cluster and field galaxies.

In Fig. 1, we compare our K-band sizes with those obtained using the H-band from the overlapping *Hubble Space Telescope* (*HST*) CANDELS survey (van der Wel et al. 2012), which covers ∼7 per cent of the UDS field. Space- and ground-based effective radii are found to be in good agreement. We find that ground-based sizes are systematically 10 per cent smaller than the
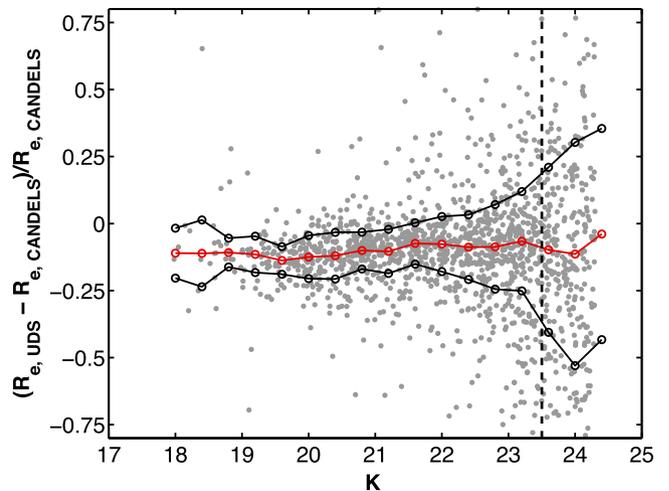
Figure 1. Relative difference between the effective-radii measured from ground-based UDS DR11 K-band imaging and *HST* CANDELS H-band imaging as a function of K-magnitude ($0.5 < z < 1.0$). The median values and median absolute deviations are displayed as red and black circles, respectively. Ground-based sizes are systematically 10 per cent smaller than the ones measures from space. This is due to both the lower background noise in space-based images and the expected variation between filters (Kelvin et al. 2012). We choose a magnitude limit of $K = 23.5$ (vertical line), which corresponds to a 25 per cent scatter, to only select reliable effective radii.

space-based ones, which is consistent with the expected variation across wavelengths (Kelvin et al. 2012). We impose a K-band cut of $K = 23.5$ (vertical line in Fig. 1) to reject faint galaxies with unreliable R_e values. This flux limit corresponds to a 25 per cent scatter in $\delta R_e/R_e$, estimated using the normalized median absolute deviation and rejects 11.5 per cent of the total sample.

After applying these quality cuts we are left with a sample of 5421 (1453) SF, 1146 (307) PAS, and 95 (26) PSB field (cluster) galaxies.

3 RESULTS

3.1 Galaxy size as a function of specific star formation rate

In Fig. 2, we show the dependence of the median R_e on SSFR for the SF galaxies in our sample. We find that R_e increases approximately linearly with log SSFR. When we split galaxies by environment, we observe that cluster galaxies with high SSFRs have larger median R_e than their field counterparts. The vertical dashed lines in Fig. 2 correspond to the approximate boundaries between the three SF sub-populations described in Section 2.3, which correlate well with SSFR. Thus, most of the galaxies with SSFR $> 10^{-9.0}$ yr^{-1} belong to the population of young SF galaxies, i.e. SF1.

In Fig. 3, we show the stellar-mass–size relation for SF1 galaxies as a function of environment. The values correspond to the median galaxy size in each mass bin, and the errorbars represent the error on the median, estimated using a bootstrapping technique. The lower mass limit corresponds to the mass completeness limit ($10^{9.0}$ M$_\odot$). The stellar-mass–size relation does not extend beyond $10^{10.5}$ M$_\odot$ because there are no SF1 galaxies with higher masses in our survey. As expected, in both environments galaxies increase in size for increasing stellar mass (Shen et al. 2003; van der Wel et al. 2014). However, it is evident that the remaining SF1 galaxies in clusters (that are not yet significantly affected by environmental quenching) are on average larger than in the field at all stellar masses. We fit
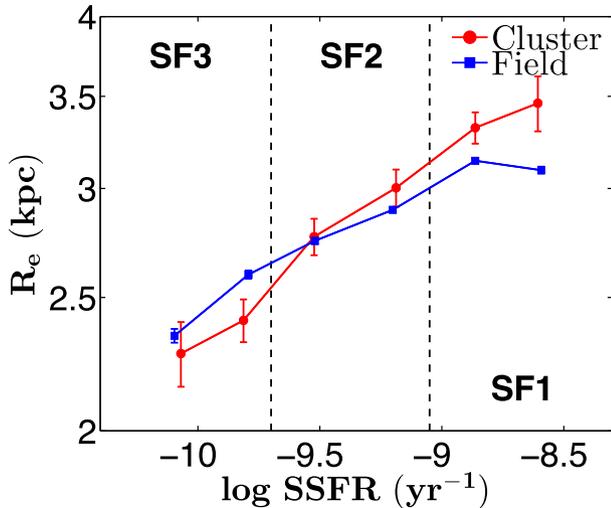
Figure 2. Median effective radius of SF galaxies as a function of SSFR at $0.5 < z < 1.0$. The red and blue lines correspond to cluster and field environments, respectively. The data points are centred on the median SSFR in each bin and the 1σ confidence error bars are estimated using bootstrapping. The vertical dashed lines delimit the regions typically occupied by the different star forming populations: SF1, SF2, and SF3, in order of decreasing mean SSFR. The SF1 galaxies (with the highest SSFR) are found to be, on average, larger in the cluster environment than in the field.
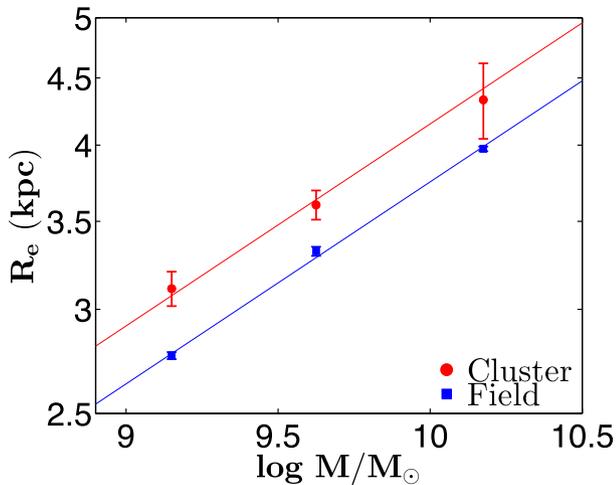
Figure 3. Stellar-mass–size relations of cluster (red) and field (blue) high-SSFR galaxies (SF1 galaxies) at $0.5 < z < 1.0$. The errorbars correspond to the 1σ confidence intervals estimated using bootstrapping. We fit a linear model to each mass–size relation (solid lines) in order to compare them. We find that cluster SF1 galaxies are systematically 9 per cent larger than their field counterparts at all masses.

a linear model with fixed slope ($\log R_{\rm e}/\log M_* = 0.154$) to the data from both environments and compare the intercepts to quantify the level of agreement. The intercept value in the cluster environment is $\log R_{\rm e}(M_* = 10^{9.5}\,{\rm M_\odot}) = 0.542 \pm 0.013$, in contrast with a field value of $\log R_{\rm e}(M_* = 10^{9.5}\,{\rm M_\odot}) = 0.498 \pm 0.002$. This represents a 3.4σ discrepancy between the cluster and field environments. We note, however, that our cluster sample contains contaminants from the field, which dilutes the differences between environments. Hence, the difference measured here is likely to be a lower limit and the real level of significance may be much higher.

In Figs 2 and 3, we have shown that the SF1 galaxies that survive in the cluster are on average larger than the general SF1 population in the field. This is unlikely to be driven by an increase in the SSFR of cluster galaxies as a result of an interaction with the cluster environment. This is because SF1 galaxies are the largest population in size ($R_{\rm e}$), on average (see Fig. 2), so increasing the SSFR of SF2 or SF3 galaxies to become SF1 galaxies would decrease the median size rather than increase it. From this, we conclude that dense environments affect the mass–size relation of young, highly SF galaxies.

3.2 A lack of compact star-forming galaxies in galaxy clusters

In this section, we examine the distributions of galaxy size and Sérsic index as a function of environment for our SF1 galaxies. We look first at the distribution of galaxies across the mass–size and mass–Sérsic index planes (left-hand and central panels of Figs 4 and 5). The first two panels on the left in Fig. 4 show the distribution of SF1 galaxies on the stellar-mass–size plane, the left-hand panel corresponds to clusters and the central one to the field. The straight line in both panels corresponds to a linear fit to the mass–size relation in the field, which we use as a reference,

$$\log R_{\rm e} = 0.202 \log M_* - 1.426. \tag{1}$$

We observe that the cluster and field distributions are notably different. The cluster distribution peaks above the field mass–size relation, indicating larger sizes at the same stellar mass. In Fig. 5, we look at the distribution of SF1 galaxies across the mass–Sérsic index plane. The dashed line corresponds to a linear fit to the field mass–n relation, which is consistent with $n = 1$. We find that the cluster distribution (left) peaks at lower values of n than in the field (centre).

In the right-hand panels of Figs 4 and 5 we compare the cluster and field distributions of n and normalized $R_{\rm e}$, i.e. removing the mass dependence of the field sample (equation 1). To remove the contaminants from the cluster sample we statistically subtract the contribution due to field galaxies that are erroneously included in the cluster sample.

The distributions of $R_{\rm e,norm}$ and n are normalized to unity to allow direct comparison of their shape. We see that the distributions of $R_{\rm e,norm}$ in high- and low-density environments are significantly different ($p_{\rm KS} = 1.2 \times 10^{-5}$). As suggested from the previous results, the cluster SF1 population is skewed towards higher $R_{\rm e,norm}$ values, as compared to the field. This galaxy population is known to be strongly depleted in dense environments (Socolovsky et al. 2018). This trend is likely to be produced by the preferential quenching of the compact SF1 galaxies. We also find a moderate but significant difference in the distribution of n between cluster and field SF1 galaxies ($p_{\rm KS} = 7.2 \times 10^{-3}$). Cluster SF1 galaxies seem to have a narrower distribution around $n = 1$, while they have slightly higher n in the field. Thus, SF1 galaxies with slightly higher n might also be preferentially quenched in clusters.

In summary, we find that the remaining SF1 galaxies in dense environments are on average larger, potentially because the compact SF1 galaxies are preferentially missing in dense environments. These compact SF1 galaxies also have higher Sérsic indices.

3.3 The cluster post-starburst mass–size relation

In Socolovsky et al. (2018), we found that PSB galaxies are the descendants of SF1 galaxies in clusters at $0.5 < z < 1.0$. We found that the stellar mass function of cluster PSBs present a very distinctive
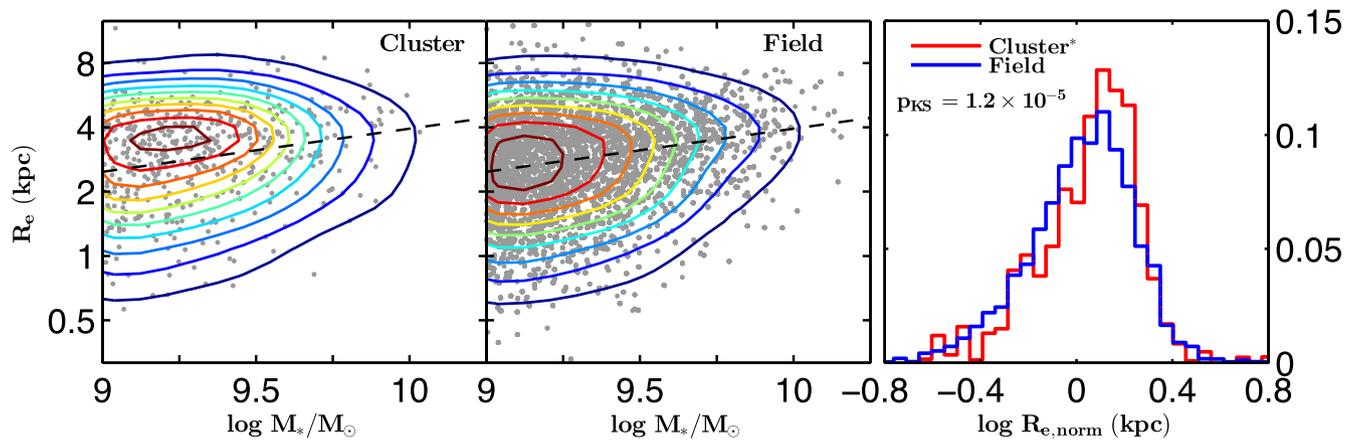
Figure 4. The stellar-mass–size relation for SF1 galaxies in the UDS at $0.5 < z < 1.0$. The grey dots represent the position of individual galaxies across the mass–size plane. The con tours show the number of galaxies per unit area on the diagram and normalized by the comoving volume of the field. The left-hand and central panels correspond to cluster and field galaxies, respectively. The black dashed line in the first two panels corresponds to the best-fitting linear model to the field population. The right-hand panel represents the distribution of the variable $R_{e,norm}$ or the ratio between the effective radius of a galaxy and the value predicted by the best-fitting model to the field data. The red line corresponds to the cluster and the blue to the field populations (note the asterisk next to the cluster label indicating it is the background-subtracted cluster sample). The field and cluster distributions are significantly different, according to a KS test (p_{KS} is quoted on the top left corner), with the cluster SF1 galaxies being, on average, larger than in the field.
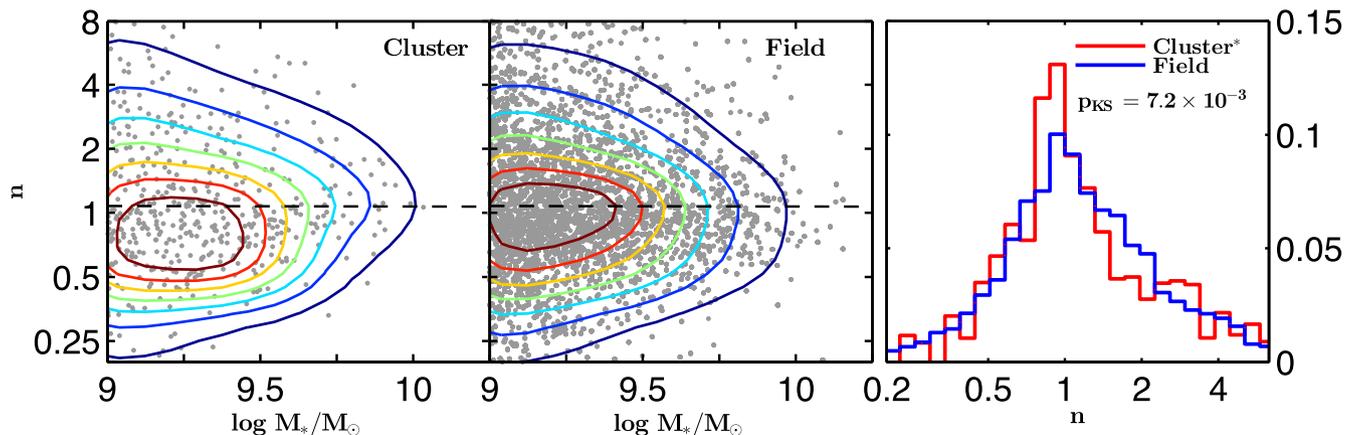
Figure 5. The stellar-mass–Sérsic index relation for SF1 galaxies in the UDS at $0.5 < z < 1.0$. The grey dots represent the position of individual galaxies across the mass–Sérsic index plane. The con tours show the number of galaxies per unit area on the diagram and normalized by the comoving volume of the field. The black dashed line in the first two panels corresponds to the best-fitting linear model to the field population. The left-hand and central panels correspond to cluster and field galaxies, respectively. The right-hand panel shows the distributions of n in clusters (red) and in the field (blue; the asterisk next to the cluster label indicates that it is the background-subtracted sample). We observe that cluster galaxies tend to have lower n values with respect to the field.

steep low-mass slope. Such a steep slope is only matched by the SF1 mass function. This implies that the only possible progenitors to PSBs are SF1 galaxies. To build on this result, we analyse the mass–size relation of PSBs to gain insight into the potential transformations that SF1 galaxies undergo as they quench in clusters.

Figs 6 and 7 show the difference between the cluster and the field SF1 galaxy distributions across the mass–size and mass–Sérsic index planes as colour con tours. Both cluster and field distributions are normalized to unity to highlight their differences. Superimposed on the con tours, the best-fitting line to the field SF1 mass–size (equation 1) and mass–n relations are presented, to aid the comparison with Figs 4 and 5.

Although PSBs in clusters are generally more compact than the average size of the SF1 galaxies, we find that the distribution of the cluster PSBs in the mass–size (Fig. 6) and mass–n (Fig. 7) planes coincides with the region where cluster SF1 galaxies are missing

with respect to the field, i.e. 48/54 of the PSBs are found below the SF1 mass–size relation of the field. Additionally, cluster PSBs typically have $n \sim 1.5$, which indicates that they partially maintain a disc-like nature. Furthermore, cluster PSBs and compact field SF1 galaxies are consistent with having the same n distribution. Therefore, we suggest that the compact SF1 galaxies undergo a gentle evolution to become PSBs in dense environments, without significant structural transformation.

4 DISCUSSION

4.1 The effect of the group environment on the star-forming population

In Section 3.2, we showed that the remaining high-SSFR galaxies (SF1 galaxies) in clusters are on average larger than the SF1 galaxies
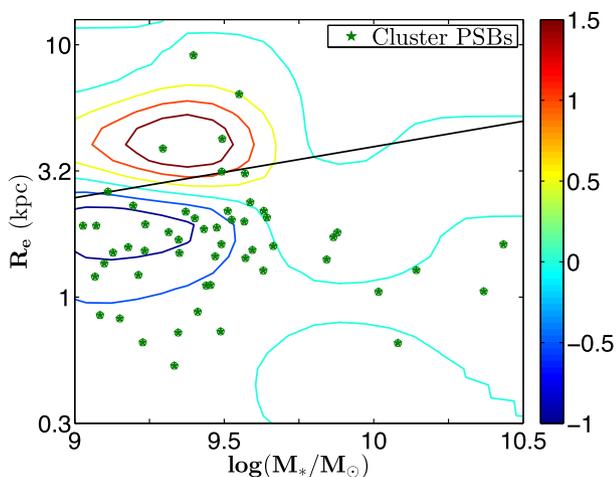
Figure 6. Comparison of mass–size relations of SF1 galaxies and PSBs in the redshift range $0.5 < z < 1.0$. The con tours represent the differential distribution of SF1 galaxies (i.e. the cluster minus the field distributions). The green stars show the location of cluster PSB galaxies. The solid line represents the mass–size relation of field SF1 galaxies for comparison. Cluster PSBs are located in the regions of the mass–size relation where SF1 galaxies are depleted in clusters with respect to the field, i.e. below the solid black line.
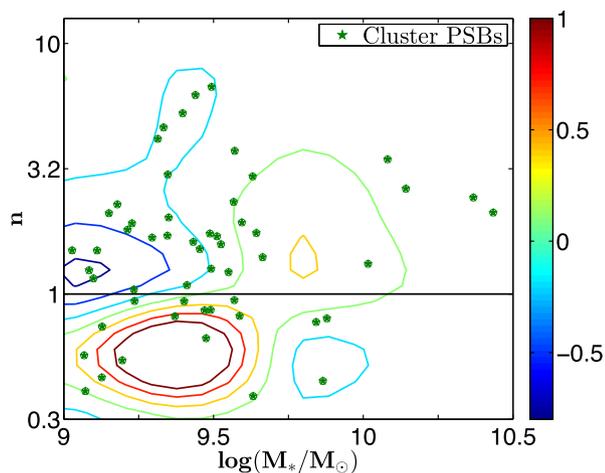
Figure 7. Comparison of mass–Sérsic index relations of SF1 galaxies and PSBs in the redshift range $0.5 < z < 1.0$. The con tours represent the differential distribution of SF1 galaxies (i.e. the cluster minus the field distributions). The green stars show the location of cluster PSB galaxies. The solid line represents the mass–Sérsic index relation of field SF1 galaxies for comparison. As in the case of the stellar mass–size relation, cluster PSBs are located in the regions where SF1 galaxies are depleted in clusters with respect to the field, in this case above the black line.

located in the field. We also show that this trend is most likely driven by a lack of SF1 galaxies with small R_e at a given stellar mass, see Figs 4 and 5. There are two plausible explanations for this observation: (1) environment affects SF1 galaxies in such way that their R_e increases; or (2) compact galaxies are being preferentially quenched in the cluster environment. We expand on these scenarios below.

Previous observational work has found that elliptical systems tend to be larger in high-density environments than in the field at $z \gtrsim 1$ (Cooper et al. 2012; Lani et al. 2013). From a theoretical point of view, this has been explained through either the

repeated interaction between galaxies (harassment) or dry mergers that take place in crowded environments (van Dokkum 2005; Oogi & Habe 2013; Shankar et al. 2013). However, major mergers and harassment are thought to disrupt galactic discs and lead to an enhancement of the bulge component (Toomre & Toomre 1972; Farouki & Shapiro 1981; Moore et al. 1996; González-García & Balcells 2005; Aceves, Velázquez & Cruz 2006). Consequently, major merging and harassment do not provide a viable explanation for the large sizes of the cluster SF1 population, which consists mainly of star-foming discs with typical Sérsic indices $n \sim 1$ (see Fig. 5). Conversely, minor galaxy mergers are thought to enable the growth of the disc component (Younger et al. 2007; Naab, Johansson & Ostriker 2009; Sil'Chenko et al. 2011). However, we expect SF1 galaxies to evolve into PSBs through environmental quenching (Socolovsky et al. 2018), and PSBs are compact. Therefore, we cannot discard the possibility of two independent processes acting simultaneously on the SF1 population: minor mergers may be responsible for the increase in size of cluster SF1 galaxies and major gas-rich mergers (e.g. between two SF1 galaxies) might be quenching them into compact PSBs (Wild et al. 2016). Note that these two processes are disconnected from each other, i.e. galaxies may undergo one of them rather than one after the other.

The main weakness of the major merger hypothesis is the observed range of Sérsic indices for both SF1 and PSB in clusters. The median Sérsic index of cluster PSBs is $n \sim 1.5$, which is low for a post-major merger scenario (González-García & Balcells 2005). Although some simulations have shown that a disc can form after a major wet merger (Athanassoula et al. 2016), the time required for this to occur is significantly longer than the expected duration of the PSB phase ($\lesssim 1$ Gyr; Wild et al. 2016; Socolovsky et al. 2018). At $z < 0.1$, PSBs have high Sérsic index values and are thought to be major merger remnants that tend to reside in low-density environments (Zabludoff et al. 1996; Blake et al. 2004; Pawlik et al. 2018). In contrast, we suggest our PSBs are originated via some kind of gentle gas removal in galaxy clusters. Hence, these results are not contradictory. On the other hand, minor mergers with dwarf galaxies that we cannot observe provide a feasible explanation. However, this may be difficult to reconcile with the observed Sérsic index of SF1 galaxies ($n \sim 1$).

Instead, we favour the hypothesis in which compact SF1 galaxies are preferentially quenched in dense environments. This naturally leads to the remaining SF1 population appearing on average larger in the cluster while the quenched galaxies (PSBs) are smaller than the typical SF1 in the field. This preferential quenching of compact objects is hard to reconcile with the environmental mechanisms previously mentioned. For example, ram-pressure stripping and tidal interactions are expected to act more efficiently in more extended galaxies, with shallower gravitational potentials so that the gas is more easily disturbed (Bothun et al. 1993; Abadi, Moore & Bower 1999; Moore et al. 1999). Scenarios involving quenching induced by galaxy mergers were also considered, but these are not expected to depend on galaxy size.

Given that purely environmental processes fail to describe our results, we suggest that the rapid environmental quenching of compact SF1 galaxies is a combination of both, internal and external mechanisms. Our hypothesis, summarized in Fig. 8, is based on a 'bathtub'-type model (Bouché et al. 2010), in which the star formation in a galaxy is regulated by the balance between gas inflows and outflows. Broadly speaking, gas in galaxies is present in two phases: a cold reservoir and hot reservoir. The cold gas reservoir (or ISM) corresponds to the dense gas typically found within the disc, and represents the instantaneous fuel for star formation. The
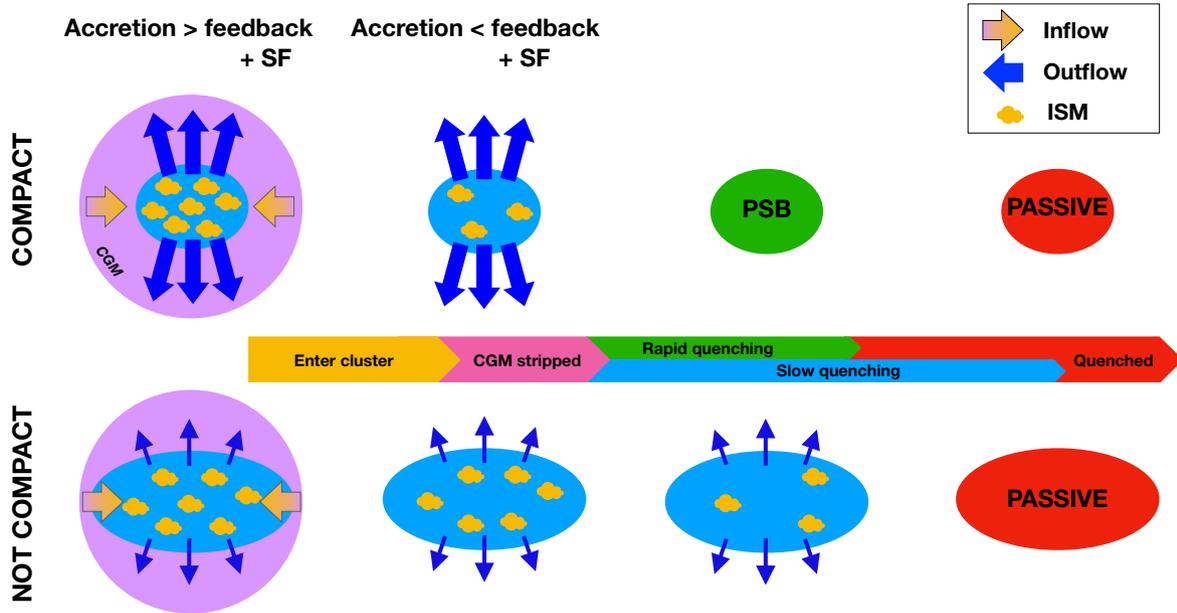
Figure 8. Diagram illustrating the different environmental quenching pathways followed by high-SSFR galaxies depending on whether they are compact (top row) or not (bottom row). The ellipses represent the location of the stars, the yellow clouds represent the ISM and the purple circles are the CGMs. The blue arrows pointing outwards from the galactic disc represent the outflows, stronger on the top sequence. The yellow arrows pointing inward represent the inflow of gas, which stops immediately as the galaxy comes in contact with the ICM. In the compact SF1 case, the strong outflows expel most of the ISM in a short time-scale, which rapidly quenches the galaxy leading to the PSB phase. Non-compact SF1 galaxies host weaker outflows, therefore they are able to sustain their star formation over a longer period of time. However, the end state for both pathways is a red, quiescent galaxy.

hot gas reservoir refers to the extended halo of diffuse gas in which the galaxy is embedded (circumgalactic medium, CGM). The gas in the CGM is too hot to collapse into stars but has the potential to cool down with time and feed the ISM through cold streams, for this reason the CGM is also referred to as the long-term gas reservoir.

The inflows (represented with yellow arrows in Fig. 8) consist of gas from the cosmic web being accreted by the galaxy. On its infall, this gas forms the CGM. As it cools down, it migrates inwards. In contrast, outflows (blue arrows in Fig. 8) send gas from the ISM back into the CGM. These outflows could be driven by stellar, supernovae, or AGN feedback. Nevertheless, the expelled gas can be recycled after some cooling time, when it is reaccreted into the ISM. However, if the galaxy becomes a satellite in a group/cluster, the CGM is largely stripped away via interaction with the ICM (Larson et al. 1980). The ICM also halts the accretion of gas from the cosmic web, so that cluster galaxies are left only with their short-term reservoir to fuel star formation. Although all galaxies have their hot gas reservoir stripped away almost instantaneously, this has no immediate effect on the ongoing star formation. Therefore, those galaxies with the highest SSFRs and/or strongest galactic outflows will deplete their cold gas reservoir faster and, consequently, quench. This scenario is similar to the 'overconsumption' process described in McGee, Bower & Balogh (2014), which is proposed to rapidly quench satellite galaxies at $z \sim 1.5$.

Some studies have found that compact galaxies are more efficient at transforming gas into stars (Young 1999). Similarly, at fixed SFR, compact in size means higher star formation surface density, which is associated with stronger outflows (Heckman, Armus & Miley 1990). In this study, we do not find higher SFRs in compact SF1 galaxies but they may host stronger stellar-wind-driven outflows. From a theoretical viewpoint, the strength of these superwinds scales with star formation rate density (Σ_{SFR}). Com-

pact SF1 galaxies have higher Σ_{SFR} due to their compact nature and the same SFR as the rest of SF1 galaxies, therefore, they are expected to produce stronger outflows (top row of Fig. 8). On the other hand, the rest of the SF1 population (i.e. not compact; second row of Fig. 8) may have more modest outflows, which would allow them to stay SF over longer time-scales before they also run out of fuel ('delayed-then-rapid' environmental quenching scenario; Wetzel et al. 2013). This theory provides a successful explanation for why compact SF1 galaxies quench faster than their more extended counterparts. They are more efficient at evacuating their cold gas reservoir after the cluster environment prevents the replenishment of gas by blocking the inflows.

In summary, stellar and supernova winds in combination with the interaction with the ICM may cause the rapid quenching predicted by Socolovsky et al. (2018) for SF1 galaxies in overdense environments. This hypothesis anticipates that environmental quenching does not trigger significant structural evolution. PSBs appear, on average, more compact than the general SF1 population because they are primarily the descendants of the compact SF1 galaxies.

This theory predicts stronger outflows in compact SF1 galaxies than in large ones. This can be tested by looking at outflow signatures in spectra of galaxies above and below the mass–size relation of the field SF1 sample.

4.2 Spectral analysis: evidence for strong outflows in compact star-forming galaxies

In this study, we find evidence that compact galaxies with high SSFR (SF1s), are more susceptible to being quenched in the cluster environment. We hypothesize that this result could be explained by a combination of both environmental and secular processes in the following scenario: (i) upon cluster infall, interaction with the ICM
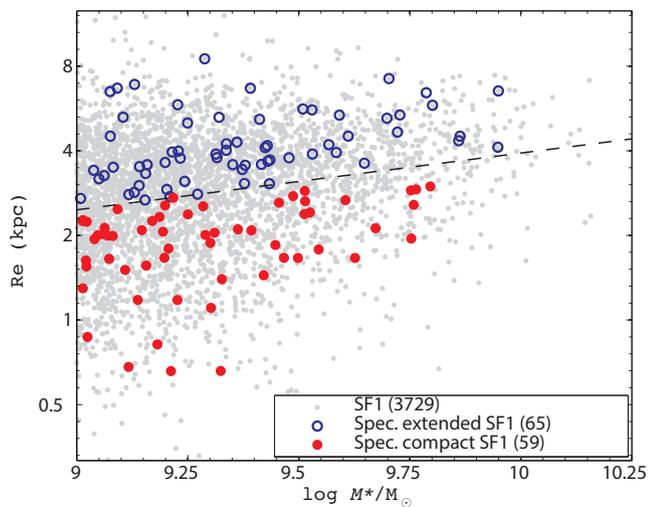
Figure 9. The stellar-mass–size relation for SF1 galaxies in the UDS field ($0.5 < z < 1$), showing the sample with available optical spectra from UDSz. The linear fit to the field mass–size relation is also shown for reference [black-dashed line; see equation (1)]. We define all galaxies with optical spectra that lie above the fit to the mass–size relation as 'extended' (blue circles), and those that lie below as 'compact' (red points). Relevant sample sizes are shown in the legend.

removes the galaxy's extended hot gas reservoir, shutting down cosmic accretion; and (ii) the strong stellar feedback in these compact galaxies causes significant outflows which rapidly expel any remaining cold gas from the central regions. This scenario would naturally lead to the rapid quenching of compact SF1 galaxies in clusters and their subsequent evolution into cluster PSBs.

To test this hypothesis we use the available deep optical spectra in the UDS field to determine whether the strong gaseous outflows required are present in our compact SF1 population. These spectra are provided by UDSz, the spectroscopic component of the UDS (ESO Large Programme 180.A-0776, PI: Almaini), which used both the VIMOS and FORS2 instruments on the ESO VLT to obtain optical spectra for >3500 galaxies in the UDS field (see Bradshaw et al. 2013; McLure et al. 2013). For our field/cluster SF1 galaxies, we find that 124 low-resolution VIMOS spectra ($R \sim 200$) are available and that these spectra are evenly distributed throughout the SF1 mass–size relation (see Fig. 9). In the following, we define all galaxies with optical spectra that lie above the fit to the mass–size relation to be 'extended', and those that lie below to be 'compact'. For these spectra, spectroscopic redshifts z_{spec} were obtained by Bradshaw et al. (2013) via EZ (Garilli et al. 2010), which uses a cross-correlation of spectral templates. Optimal solutions were also confirmed using spectral line identification in SGNAPS (Paioro & Franzetti 2012). In this work, we use these redshifts to shift the individual galaxy spectra to their respective rest frame (i.e. systemic frame).

In order to determine the presence of gaseous outflows, we use the Mg II absorption doublet ($\lambda\lambda$ 2796, 2803 Å), which is a sensitive tracer of low-ionization interstellar gas. The detection of a blueshifted component to this absorption feature is generally indicative of galactic-scale outflows along the line-of-sight to the observer. Unfortunately, the S/N in the VIMOS spectra is not sufficient to reliably determine the structure of the Mg II profile on an individual galaxy basis. We therefore increase the effective S/N via a stacking analysis, combining the individual rest-frame spectra following an optimised flux normalization. For this, we generate two median-stacked spectra: (i) a red-optimized stack ($\lambda > 3500$ Å), using a flux normalization over the Balmer break region; and (ii) a blue-optimized stack ($\lambda < 3700$ Å), using a flux normalization over the Mg II continuum. For the blue-optimized stack, we also apply an upper 2σ clip to individual spectra that deviate from the median flux within the Mg II region ($2775 < \lambda < 2825$ Å). This clipping removes a handful of spectra (< 10 per cent) that exhibit Mg II emission, which would otherwise bias our stacking analysis. The final median-stacked spectrum is a splice of the red- and blue-optimized stacks. The median-stacked spectra for both our 'extended' and 'compact' SF1 galaxies are shown in Fig. 10.

For both our median stacks, we also perform a full spectral fit (stellar component plus gas emission lines) using the penalized pixel-fitting method (PPXF; Cappellari & Emsellem 2004; Cappellari 2017) and the MILES spectral templates (Vazdekis et al. 2010). Note that due to the range of these spectral templates, our PPXF fits are limited to $\lambda > 3540$ Å (see Fig. 10). We find that our median-stacks are well modelled by the resultant spectral fits, which also clearly demonstrate that several spectral features (e.g. Balmer lines, [O II], [O III]) are all well centred with respect to their expected wavelengths. For Mg II, this indicates that an observed offset $\Delta\lambda$ from the systemic-frame wavelength ($\lambda\lambda$ 2796, 2803 Å) is unlikely to be introduced by any uncertainty in our stacking procedure or individual spectroscopic redshifts. Consequently, this suggests that if such offset is observed, it will be related to a genuine velocity offset Δv in the relevant absorbing gas from the systemic redshift, and therefore imply the presence of galactic-scale outflows.

In Fig. 10, an initial comparison of our median stacks reveals a significant difference in the nature of the Mg II absorption between our compact and extended SF1 galaxies. With respect to the central systemic-frame wavelength of the Mg II doublet (λ2799.5 Å), for extended SF1s the absorption profile is well-centred, while for compact SF1s there is a clear offset towards bluer wavelengths. To determine the significance of this potential offset, we use the following procedure. We model the Mg II absorption profile using a single component, consisting of a Gaussian-convolved doublet with a free centroid wavelength. The doublet itself has a fixed line ratio (i.e. 1.1:1; as observed for high-z SF galaxies; Weiner et al. 2009) and an intrinsic narrow width for each line. In the fitting process, this doublet is convolved with a Gaussian to model the instrument response, which is necessary since the Mg II doublet is unresolved in our low-resolution spectra. The Gaussian used for convolution is either fixed to the FWHM of the O II emission, or left as a free component in the fit (both cases of which yield consistent results in this study). This simple model yields the offset $\Delta\lambda$ of the Mg II doublet with respect to the systemic-frame wavelength, which can be used to determine a characteristic velocity offset Δv from the systemic redshift. For our stacked spectra, this velocity offset represents an estimate of the typical outflow velocity in the low-ionization gas for our galaxy populations. The 1σ uncertainties in these velocity measurements are determined using the variance between analogous fits performed on 1000 simulated spectra generated via a bootstrap analysis.

For our 'extended' and 'compact' SF1 galaxies, the relevant fits to the Mg II profile are presented in Fig. 10. In each case, we determine the velocity offset Δv of the Mg II absorption profile with respect to the systemic redshift. In the case of extended SF1 galaxies, we find this velocity offset to be minimal ($\Delta v = 40 \pm 36$ km s^{-1}). This indicates that no significant outflowing (i.e. blue-shifted) component of low-ionization gas is present in these galaxies. However, for compact SF1 galaxies, we find a significant excess of blue-shifted absorption indicative of gaseous outflows. In this case, our best-fitting
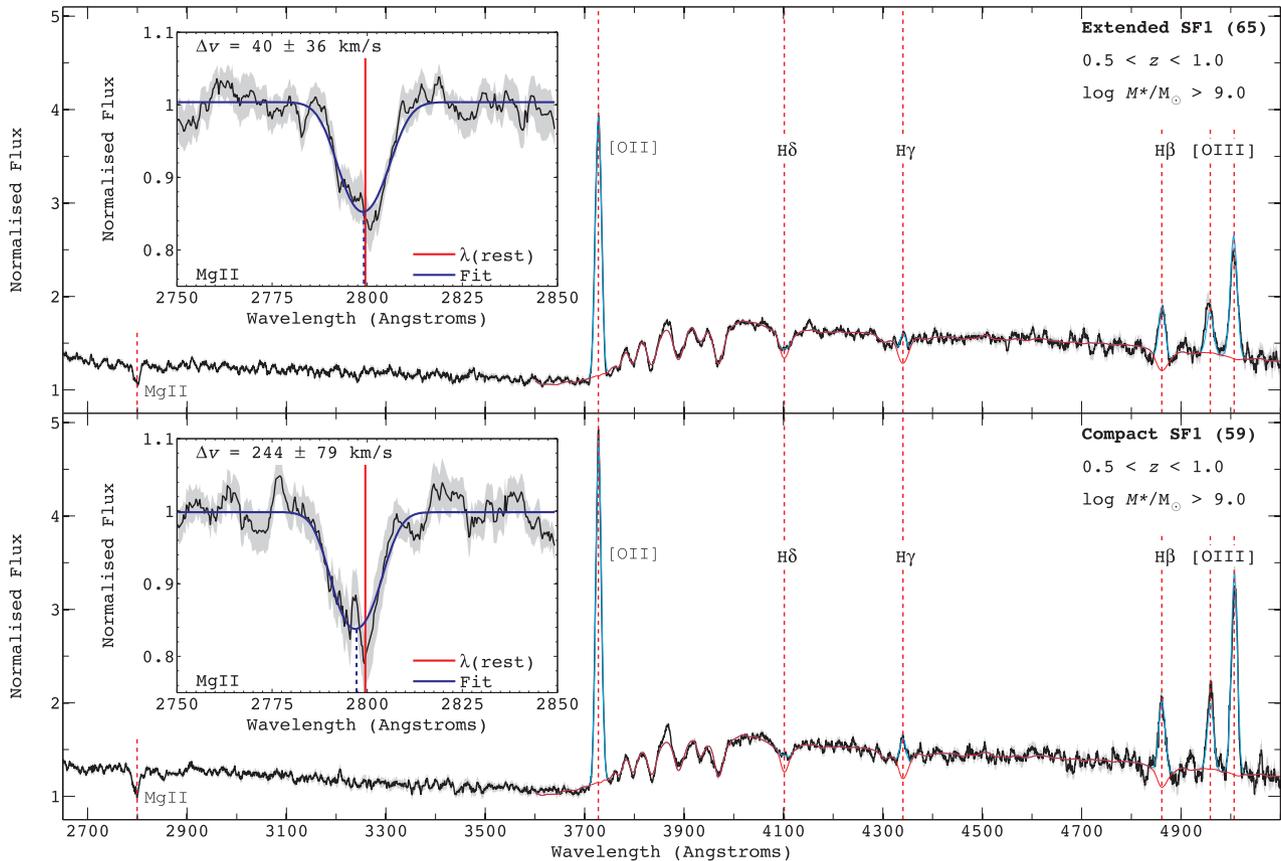
Figure 10. Stacked optical spectra for 'extended' and 'compact' SF1 galaxies in the UDS field at $0.5 < z < 1$. Top panel: a stacked optical spectrum for extended SF1 galaxies (i.e. those that lie above the fit to the mass–size relation in Fig. 9). For reference, we also show the full spectral fit obtained from PPXF for both the stellar component (red line) and the gas emission lines (cyan lines). Bottom panel: an analogous stacked spectrum and PPXF fit for compact SF1 galaxies (i.e. those that lie below the fit to the mass–size relation in Fig. 9). Relevant sample sizes are shown in the legend. In each case, the sub-panel shows the best fit to the Mg II absorption profile, using a model comprising a single Gaussian-convolved doublet with a free centroid. The central rest-frame wavelength of the Mg II doublet ($\lambda 2799.5$ Å; red line) and corresponding offset in the best fit ($\Delta\lambda$; blue-dashed line) is shown for reference. These fits yield the typical velocity offset Δv of the Mg II doublet from the systemic redshift. For extended SF1 galaxies, we find this velocity offset to be minimal ($\Delta v = 40 \pm 36\,\mathrm{km\,s^{-1}}$). In contrast, for compact SF1 galaxies, we require a more significant blue-shift in the doublet to explain the structure of the Mg II profile, and therefore a stronger velocity offset ($\Delta v = 244 \pm 79\,\mathrm{km\,s^{-1}}$). These results imply the presence of stronger galactic-scale outflows in more compact SF1 galaxies.

model yields a significant velocity offset in the Mg II absorption profile ($\Delta v = 244 \pm 79\,\mathrm{km\,s^{-1}}$). This indicates that the strong stellar feedback inherent to these compact SF galaxies is likely causing strong galactic-scale outflows or winds in their interstellar medium. Finally, we note that more complex models involving two components (e.g. one fixed at the rest-frame wavelength for the systemic absorption, and another with a free centroid to model the outflow; see e.g. Bradshaw et al. 2013) were also explored, and that these all yield consistent results, to within the fit uncertainties. We also note that in each case, the use of either median- or mean-stacked spectra in our analysis leads to consistent Mg II profiles and Δv measurements, and has no significant impact on the results of this study.

Taken together, these results indicate that strong galactic-scale outflows are commonplace in compact SF1 galaxies, but not a significant factor in the more extended SF1 galaxies. This supports our hypothesis that when SF1 galaxies infall to the cluster environment and have their extended gas reservoirs removed by ICM interactions, the subsequent evolution is strongly dependent on the compactness of the galaxy. For extended galaxies, the lack of strong outflows leads to the galaxy retaining its cold gas disc and therefore

the continuation of star formation. In contrast, for compact galaxies the stronger outflows present will quickly lead to the removal of the remaining cold gas disc, which would result in the rapid quenching of star formation and the subsequent evolution of these galaxies into cluster PSBs.

5 CONCLUSIONS

We present the first evidence that the structure of galaxies with high SSFRs (SF1s) differs with environment at $0.5 < z < 1.0$. Using K-band structural parameters available for the UDS, we find that high-SSFR galaxies in clusters are typically larger than analogous galaxies in the field. In recent work, we found that these galaxies are strongly depleted in dense environments and undergo rapid quenching to become cluster PSBs (see Socolovsky et al. 2018). We therefore suggest that the observed difference in size is caused by the preferential quenching of compact galaxies in dense environments. We summarize our main findings as follows:

(i) Using the mass–size relation, we find that galaxies with high SSFR in the cluster environment are on average larger than their counterparts in the field.

(ii) Examining the distribution of effective radii R_e, we find that the difference in size is likely to be driven by a lack of compact SF1 galaxies in clusters. This suggests a preferential environmental quenching of the most compact galaxies. From a similar analysis of the distribution in Sérsic indices, we infer that the missing compact SF1 galaxies had higher Sérsic index, n, than the typical SF1 galaxy in the field.

(iii) We find that the structural parameters of the missing compact SF1 galaxies are compatible with those of the cluster PSB population. Building on the work of Socolovsky et al. (2018), this suggests that compact SF1s are the main progenitors of cluster PSBs, rather than the SF1 population as a whole. These galaxies are rapidly quenched and evolve into the PSB population with no significant structural evolution.

Taken together, these results indicate that rapid quenching within clusters is size dependent at $0.5 < z < 1.0$. This may explain why cluster PSBs are significantly smaller than the typical SF1 galaxy or indeed the general SF population (Maltby et al. 2018).

Regarding the quenching mechanisms, we suggest that the most likely scenario combines secular and environmental processes. The interaction with the ICM blocks the inflow of gas into the galaxy, which results in the exhaustion of the gas reservoir through star formation and outflows. Therefore, compact SF1 galaxies, which have higher surface star formation densities (similar SFR in a smaller radius), rapidly run out of fuel due to their stronger outflows. This hypothesis is supported by the spectroscopic data available for 124 of the SF1 galaxies. The spectra show evidence that the Mg II absorption feature contains a significant blue-shifted component, indicative of outflows, in those galaxies that lie below the field SF1 mass–size relation in comparison to those above it. This provides evidence supporting our model, suggesting that compact SF1 galaxies tend to host stronger galactic outflows.

In conclusion, we find evidence for size-dependent environmental quenching in clusters at $0.5 < z < 1.0$. Our results show that compact SF galaxies are preferentially and rapidly quenched in clusters to become PSBs.

REFERENCES

Abadi M. G., Moore B., Bower R. G., 1999, MNRAS, 308, 947

Aceves H., Velázquez H., Cruz F., 2006, MNRAS, 373, 632

Almaini O. et al., 2017, MNRAS, 472, 1401

Athanassoula E., Rodionov S. A., Peschken N., Lambert J. C., 2016, ApJ, 821, 90

Baldry I. K., Balogh M. L., Bower R. G., Glazebrook K., Nichol R. C., Bamford S. P., Budavari T., 2006, MNRAS, 373, 469

Baldry I. K. et al., 2012, MNRAS, 421, 621

Balogh M. L., Morris S. L., Yee H. K. C., Carlberg R. G., Ellingson E., 1997, ApJ, 488, L75

Bamford S. P. et al., 2009, MNRAS, 393, 1324

Barden M., Häußler B., Peng C. Y., McIntosh D. H., Guo Y., 2012, MNRAS, 422, 449

Blake C. et al., 2004, MNRAS, 355, 713

Bothun G. D., Schombert J. M., Impey C. D., Sprayberry D., McGaugh S. S., 1993, AJ, 106, 530

Bouché N. et al., 2010, ApJ, 718, 1001

Bradshaw E. J. et al., 2013, MNRAS, 433, 194

Brammer G. B., van Dokkum P. G., Coppi P., 2008, ApJ, 686, 1503

Bruzual G., Charlot S., 2003, MNRAS, 344, 1000

Cappellari M., 2017, MNRAS, 466, 798

Cappellari M., Emsellem E., 2004, PASP, 116, 138

Cebrián M., Trujillo I., 2014, MNRAS, 444, 682

Chabrier G., 2003, PASP, 115, 763

Cooper M. C. et al., 2012, MNRAS, 419, 3018

Drory N. et al., 2009, ApJ, 707, 1595

Faber S. M., 1973, ApJ, 179, 423

Farouki R., Shapiro S. L., 1981, ApJ, 243, 32

Furusawa H. et al., 2008, ApJS, 176, 1

Garilli B., Fumana M., Franzetti P., Paioro L., Scodeggio M., Le Fèvre O., Paltani S., Scaramella R., 2010, PASP, 122, 827

González-García A. C., Balcells M., 2005, MNRAS, 357, 753

Gunn J. E., Gott J. R., III, 1972, ApJ, 176, 1

Hartley W. G. et al., 2013, MNRAS, 431, 3045

Heckman T. M., Armus L., Miley G. K., 1990, ApJS, 74, 833

Kelkar K., Aragón-Salamanca A., Gray M. E., Maltby D., Vulcani B., De Lucia G., Poggianti B. M., Zaritsky D., 2015, MNRAS, 450, 1246

Kelvin L. S. et al., 2012, MNRAS, 421, 1007

Lani C. et al., 2013, MNRAS, 435, 207

Larson R. B., Tinsley B. M., Caldwell C. N., 1980, ApJ, 237, 692

Maltby D. T. et al., 2010, MNRAS, 402, 282

Maltby D. T. et al., 2016, MNRAS, 459, L114

Maltby D. T., Almaini O., Wild V., Hatch N. A., Hartley W. G., Simpson C., Rowlands K., Socolovsky M., 2018, MNRAS, 480, 381

McGee S. L., Bower R. G., Balogh M. L., 2014, MNRAS, 442, L105

McLure R. J. et al., 2013, MNRAS, 428, 1088

Moore B., Katz N., Lake G., Dressler A., Oemler A., 1996, Nature, 379, 613

Moore B., Lake G., Quinn T., Stadel J., 1999, MNRAS, 304, 465

Moutard T. et al., 2016, A&A, 590, A103

Moutard T., Sawicki M., Arnouts S., Golob A., Malavasi N., Adami C., Coupon J., Ilbert O., 2018, MNRAS, 479, 2147

Muzzin A. et al., 2013, ApJ, 777, 18

Naab T., Johansson P. H., Ostriker J. P., 2009, ApJ, 699, L178

Oogi T., Habe A., 2013, MNRAS, 428, 641

Paioro L., Franzetti P., 2012, Astrophysics Source Code Library, record ascl:1210.005

Papovich C. et al., 2012, ApJ, 750, 93

Pawlik M. M. et al., 2018, MNRAS, 477, 1708

Peng Y.-j. et al., 2010, ApJ, 721, 193

Peng C. Y., Ho L. C., Impey C. D., Rix H.-W., 2002, AJ, 124, 266

Pozzetti L. et al., 2010, A&A, 523, A13

Sérsic J. L., 1968, Atlas de Galaxias Australes. Observatorio Astronomico, Cordoba, Argentina

Shankar F., Marulli F., Bernardi M., Mei S., Meert A., Vikram V., 2013, MNRAS, 428, 109

Shen S., Mo H. J., White S. D. M., Blanton M. R., Kauffmann G., Voges W., Brinkmann J., Csabai I., 2003, MNRAS, 343, 978

Sil'Chenko O. K., Chilingarian I. V., Sotnikova N. Y., Afanasiev V. L., 2011, MNRAS, 414, 3645

Simpson C. et al., 2012, MNRAS, 421, 3060

Simpson C., Westoby P., Arumugam V., Ivison R., Hartley W., Almaini O., 2013, MNRAS, 433, 2647

Socolovsky M., Almaini O., Hatch N. A., Wild V., Maltby D. T., Hartley W. G., Simpson C., 2018, MNRAS, 476, 1242

Tomczak A. R. et al., 2014, ApJ, 783, 85

Toomre A., Toomre J., 1972, ApJ, 178, 623

Ueda Y. et al., 2008, ApJS, 179, 124

van der Wel A., Holden B. P., Zirm A. W., Franx M., Rettura A., Illingworth G. D., Ford H. C., 2008, ApJ, 688, 48

van der Wel A. et al., 2012, ApJS, 203, 24

van der Wel A. et al., 2014, ApJ, 788, 28

van Dokkum P. G., 2005, AJ, 130, 2647

Vazdekis A., Sánchez-Blázquez P., Falcón-Barroso J., Cenarro A. J., Beasley M. A., Cardiel N., Gorgas J., Peletier R. F., 2010, MNRAS, 404, 1639

Weiner B. J. et al., 2009, ApJ, 692, 187

Wetzel A. R., Tinker J. L., Conroy C., van den Bosch F. C., 2013, MNRAS, 432, 336

Wild V. et al., 2014, MNRAS, 440, 1880

Wild V., Almaini O., Dunlop J., Simpson C., Rowlands K., Bowler R., Maltby D., McLure R., 2016, MNRAS, 463, 832

Yang X., Mo H. J., van den Bosch F. C., 2009, ApJ, 695, 900

Younger J. D., Cox T. J., Seth A. C., Hernquist L., 2007, ApJ, 670, 269

Young J. S., 1999, ApJ, 514, L87

Zabludoff A. I., Zaritsky D., Lin H., Tucker D., Hashimoto Y., Shectman S. A., Oemler A., Kirshner R. P., 1996, ApJ, 466, 104

This paper has been typeset from a TEX/LATEX file prepared by the author.